Jurnal Teknologi Reaktor Nuklir

Tri Dasa Mega

Journal homepage: https://ejurnal.brin.go.id/tridam

A Probabilistic Approach to Assess Sediment Ejecta Hazard for Nuclear Power Plant Siting: Insights from the Serpong Case Study

Akhmad Muktaf Haifani[1,2], Hadi Suntoko[2], Topan Setiadipura[2], Widjojo A. Prakoso[1]

[1] *Faculty of Engineering, Department of Civil Engineering, University of Indonesia, Depok, West Java, Indonesia.*
[2] *Centre for Research of Nuclear Reactor Technology National Research and Innovation Agency Serpong, Indonesia*

ARTICLE INFO

Article history:

Received: November 6, 2025
Received in revised form: Nov. 30, 2025
Accepted: December 30, 2025

Keywords:

Probabilistic EPI
Liquefaction hazard
Sediment ejecta
Core pressure
Hydro-mechanical boundary
Nuclear site safety

A B S T R A C T

Liquefaction-induced sediment ejecta endanger the safety of nuclear power plant (NPP) sites, yet traditional indices like LPI and LSN ignore important underlying mechanisms. This paper introduces the Probabilistic Ejecta Potential Index Analysis (Prob_EPI), a physics-based alternative that takes into consideration pore pressure dynamics, interlayer effects, and hydraulic gradients. When normalized against a Hydro-Mechanical Boundary (HMB) and confirmed with six statistical measures, the 80% artesian gradient is found as the essential threshold. When applied to two boreholes (DH11 and DH17) at the proposed Serpong NPP site under 250-5000-year seismic scenarios, Prob_EPI increases with seismic strength and reveals vulnerable sand layers at depths of 5-22 m. The approach strengthens the basis for evaluating ejecta hazards and increases confidence in nuclear site selection.

1. INTRODUCTION

The emergence of sediment ejecta on the ground surface is primarily driven by the dissipation of excess pore water pressure (u_e) that develops during seismic shaking, often occurring minutes after the ground motion ceases [1-2] A well-documented case was reported by Ambraseys and Sarma during the 1964 Niigata Earthquake (Mw 7.6), where ground fissures formed 2–3 minutes after shaking onset, followed by the upward surge of water-sediment mixtures reaching 1.5 meters above the surface, transporting fluidized material from depths of 4.5 to 6.0 meters [3]. Seed further emphasized that once the excess pore pressure approaches the overburden stress, upward flow can be triggered even after cyclic loading has ceased [4].

The modelling of liquefaction-induced ground failure has evolved significantly by introducing an empirical framework that correlates liquefaction potential with the thickness of non-liquefiable surface layers and peak ground acceleration (PGA). This foundational concept was extended to develop semi-empirical procedures incorporating in-situ penetration data from the Standard Penetration Test (SPT) and Cone Penetration Test (CPT) to assess soil resistance against liquefaction. The Equivalent Shear Stress Analysis (ESA) method has been widely used to model layered soil response to dynamic loading.. The influence of interlayer interactions on pore pressure buildup and ejecta dynamics has been well documented[3]. In addition, accurate liquefaction

* Corresponding author
Email:akhm020@brin.go.id
DOI: 10/55981.tdm.2025.12936

vulnerability assessments in stratified deposits require dynamic stratigraphic calibration [4].

Conventional metrics such as the Liquefaction Potential Index (LPI) and Liquefaction Severity Number (LSN) [5] are widely applied to estimate the severity of surface manifestations of liquefaction. While these indices provide practical utility, they exhibit fundamental limitations. First, both rely on vertically aggregated scoring schemes that do not explicitly account for the depth-wise distribution of excess pore water pressure. Second, they neglect the hydraulic mechanisms associated with sediment ejecta, which are critical to understanding surface expression. Third, these approaches do not incorporate seismic–geotechnical uncertainties in a probabilistic framework [6]. Moreover, both LPI and LSN operate on a layer-by-layer basis and fail to consider interlayer interactions or vertical hydraulic gradients, which can induce artesian flows toward the ground surface [7]. The Liquefaction Demand (LD) parameter derived from CPT data has proven to be more representative in assessing the severity of sediment ejecta than conventional approaches such as LPI and LSN, as it directly accounts for the upward hydraulic pressure that triggers artesian flow and its interaction with the strength of the overlying crust layer [8]. Beyond these conceptual drawbacks, field performance data also reveal quantitative biases. Maurer et al. [7] reported that LPI underpredicted liquefaction ejecta in Christchurch, with misclassification rates exceeding 30%. In contrast, LSN tends to be overly conservative, overestimating severity in more than 25% of case histories [9]. These findings highlight the need for indices that explicitly integrate hydraulic gradients, interlayer interactions, and probabilistic uncertainty—elements that are central to developing more reliable liquefaction hazard metrics. A precise assessment of liquefaction and ejecta threats is essential for nuclear safety and adherence to international site safety standards when evaluating nuclear power plant (NPP) sites. Traditional deterministic indices frequently aren't able to capture the combined influence of mechanical and hydraulic variables that control liquefaction behavior. In order to give NPP siting decisions a more safety-consistent and credible fundamental basis, a probabilistic framework that measures these uncertainties is necessary.

To overcome these limitations, more recent methods such as the Artesian Flow Potential (AFP) and Ejecta Flow Index (EFI) have been introduced to account for artesian-driven fluid pressures—essentially, excess hydraulic head that can force sediment upward to the ground surface [6]. Field observations from Christchurch provide compelling support for this idea, showing that local hydraulic gradients, fractures within the non-liquefiable crust, and the sustained presence of excess pore water pressure all contribute significantly to the development of ejecta [5]. Surface ejecta spatial patterns have been found to be significantly related to subsurface artesian flow routes, implying that upward water movement is important in ejecta generation [3]. To supplement this viewpoint, post-liquefaction modeling approaches that replicate the interaction of pore water and sediment across stratified soil profiles have been identified as critical for capturing the real dynamics of ejecta transport [10,11]. Based on these conceptual advances, the Ejecta Potential Index (EPI) was developed to provide a quantitative representation of sediment ejecta severity. This index incorporates not only the peak values of excess pore water pressure, but also its persistence over time once it exceeds the critical hydraulic gradient required to generate upward flow.

This study proposes the concept of probabilistic liquefaction based on the Ejecta Probability Index (Prob_EPI) as the ratio between EPI and HMB, where the Hydraulic Mechanical Boundary (HMB) is delineated based on the threshold vertical-to-horizontal hydraulic gradient ratio (H:V = 1:1), corresponding to 80% of the maximum pore water pressure influence. Conceptually, the HMB represents a subsurface interface zone where upward hydraulic forces—such as excess pore pressure and vertical seepage gradients—interact with the mechanical response of saturated sandy soils, including effective stress and deformation behavior [11]. In this study, the HMB is defined as an imaginary vertical line extending from the phreatic surface to a depth of 30 m, marking the maximum extent of artesian influence within the geotechnical domain. For robustness, both the delineation of HMB and the computation of Prob_EPI were validated using a multi-method framework—comprising Cross-Correlation, Dynamic Time Warping (DTW), Area Difference, Kullback–Leibler Divergence (KLD), and Hellinger Distance—designed to minimize aleatory and epistemic uncertainties [3,5,11]. This integrative framework is expected to overcome the limitations of traditional liquefaction severity indices such as LPI and LSN by offering a more spatially and hydraulically consistent delineation of high-risk zones.

Importantly, this research is directly in line with international safety regulations. Both the International Atomic Energy Agency [12] and the United States Nuclear Regulatory Commission [13] emphasize that seismic liquefaction hazards must be evaluated using methods that explicitly incorporate uncertainty and site-specific hydraulic behavior. Inaccurate indices such as LPI and LSN can lead in either an inaccurate assessment of hazard, compromising nuclear safety, or an overestimation, causing in the justified exclusion from potential sites. This paper introduces Prob_EPI, which provides a more reliable and safety-consistent methodology for assessing liquefaction-induced ejecta hazards, particularly in the context of nuclear facility site selection and safety assessment.

Furthermore, the new IAEA Site Evaluation for Nuclear Installations [12] mandates that potential cumulative impacts like earthquake-induced liquefaction and ground deformation be reviewed and probabilistically assessed on a regular basis to assure long-term nuclear safet. Previous research, like as Katona [14], have shown that, despite progress in deterministic assessment at the Pakistan NPP, a unified probabilistic technique for beyond-design-basis liquefaction evaluation is still lacking. The current study addresses this gap by presenting a probabilistic framework that incorporates hydraulic-mechanical interactions and uncertainty quantification using the Prob_EPI approach.

2. SITE STUDY

The research area its surrounding areas measuring 5 km x 5 km, with a geographical position of within the coordinates 6°19′30″S, 106°38′24″E to 6°22′12″S, 106°41′06″E. Topographically, the study area is located at an altitude between 44 m to 88 m above the average sea level. The research area is included in Cisauk subdistrict, Tangerang regency, Setu subdistrict, South Tangerang city of Banten province. Figure 1 illustrates the location of the Serpong site within the southwestern Jakarta Basin and the positions of boreholes DH11 and DH17 used for this study.

Geotechnical and geophysical investigations at the prospective Serpong NPP site have revealed that the stratigraphic conditions are composed of the Serpong Formation at the top, which consists of topsoil, clay (soft-stiff), and loose to dense sand, and the Bojongmanik Formation below, which is dominated by sandy claystone, clayey sandstone, and clastic limestone inserts with layer thicknesses ranging from 0.2-2.5 m. The cross-hole test yielded a shear wave velocity Vs30 of 268 m/s and an average SPT of 40.6, classifying the area as Type 3 (moderate) Soil per the NEHRP standards. Microtremor array measurements revealed a Vs value of 750 m/s at a depth of approximately 390 meters, showing the depth of the seismic bedrock. Earthquake hazard calculations show a maximum ground acceleration (PGA) of 0.16 g for a 1000-year return period and 0.23 g for 10,000 years at a foundation depth of about 7.5 meters, emphasizing the importance of considering liquefaction potential and layer stability when designing this strategic site structure. The study analyzes borehole data from two sites in Serpong, Indonesia—DH11 and DH17—each with detailed SPT, CPT, and Vs profiles. Site-specific geotechnical parameters were extracted from field investigations and correlated using established empirical methods. Key parameters include relative density (Dr), void ratio (e_0), shear modulus at small strain (Go), contraction rate (hpo), lateral earth pressure coefficient (Ko), over consolidation ratio (OCR), and permeability (k). Tables 1 and 2 summarize the input properties for both sites.

Table 1. Site Parameters – DH11

Depth (m)	Soil Name	Soil Type	Model	DR (%)	Go (kPa)	P (gr/cm^3)	k (m/s)	eo	NSPT	Vs (m/s)	FC (%)
0.2 -2.8	Clayey Sand	SC	PM4Sand	61.92	1021.97	1.73	0.0059	0.614	12	232.216	37.3
2.8 - 6	Sand	SP	PM4Sand	46.425	2009.02	1.73	0.0000213	0.661	12	264.802	37.3
6 - 8.8	Sand	SP	PM4Sand	45.748	2258.12	1.73	0.0000139	0.663	17	362.137	37.3
8.8 - 14.8	Gravelly Sand	SW	PM4Sand	0.822	967.75	2.04	0.001	0.798	39	369.029	17.64
14.8-24	Clayey Sand	SC	PM4Sand	0.584	990.77	2.04	0.001	0.797	41	409.406	17.64
24 - 26.8	Silty Clay	CL	PM44Silt	0.722	859.28	2.04	0.004	0.798	54	355.021	17.64
26.8 - 30	Silty Clay	CL	PM44Silt	1.104	1277.49	2.04	0.004	0.797	37	406.531	17.64

Table 2. Site Parameters – DH17

Depth (m)	Soil Name	Soil Type	Model	DR (%)	Go (kPa)	P (gr/cm^3)	k (m/s)	eo	NSPT	Vs (m/s)	FC
0 - 2.6	Silty Clay	CL	PM4Sand	69.66	890.143	1.835	0.003939394	0.591	4	159.671	88.88
2.6 - 5.6	Sandy Clay	CH	PM4Sand	0.547	1229.884	1.835	2.32935E-05	0.636	4	159.671	88.88
5.6 - 8.2	Gravelly Sand	SW	PM4Sand	0.408	1605.670	1.835	4.04834E-05	0.678	13	239.731	98.44
8.2 - 9.6	Clayey Sand	SC	PM4Sand	0.515	1580.051	1.835	0.0000020	0.646	19	273.243	98.44
9.6 – 11	Clayey Sand	SC	PM4Sand	0.624	754.766	1.835	0.01	0.613	15	251.856	98.44
11 – 14	Gravelly Sand	SW	PM4Sand	0.555	681.483	1.937	0.01	0.634	31	323.487	98.44
14 - 17	Gravelly Sand	SW	PM4Sand	0.799	942.547	1.937	0.01	0.560	8	202.778	98.44
17 – 20	Clayey Sand	SC	PM4Sand	0.406	530.551	1.937	0.01	0.678	39	350.134	98.44
20 – 23	Sandy Clay	CH	PM44Silt	0.897	1050.586	2.039	0.01	0.531	47	373.401	98.44
23 – 30	Silty Clay	CL	PM44Silt	0.987	1148.899	2.039	0.01	0.504	21	159.671	88.88

To supplement these facts, Table 3 presents the main geotechnical metrics acquired from both boreholes. This summary provides simple to distinguish between DH11 and DH17 and supports with the subsequent probabilistic EPI analysis, while also ensuring that international readers grasp the site conditions.

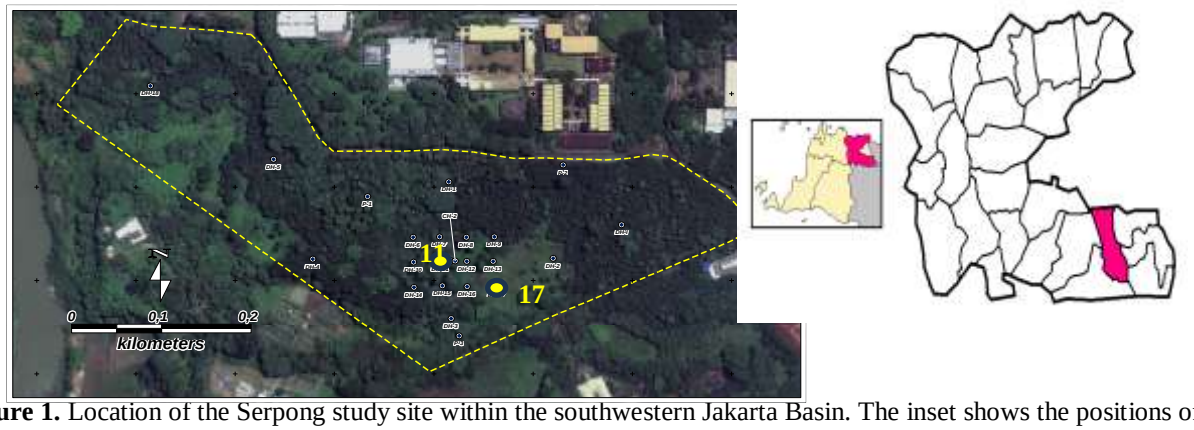

Figure 1. Location of the Serpong study site within the southwestern Jakarta Basin. The inset shows the positions of boreholes DH11 and DH17 used for Prob_EPI validation [15].

Table 3. Representative Geotechnical Parameters from DH11 and DH17 (Serpong Site)

Borehole	Vs30 (m/s)	Average NSPT	Shear Modulus Go (kPa)	Permeability k (m/s)	Dominant Soil Classification
DH11	268	40.6	~1,400 – 2,200	10^{-2} – 10^{-5}	Clayey Sand, Sand, Gravelly Sand, Silty Clay
DH17	265*	21.3	~900 – 1,600	10^{-2} – 10^{-5}	Silty Clay, Sandy Clay, Gravelly Sand, Clayey Sand

*Note: Vs30 for DH17 is estimated from the shear wave velocity profile; both boreholes indicate a moderate soil type (NEHRP Site Class D).

Table 3 presents two typical boreholes (DH11 and DH17) for the Serpong site. While these boreholes are critical input for the probabilistic EPI assessment, they may not reflect the geographic diversity of subsurface conditions throughout the area. The goal of this work is to demonstrate the approach for probabilistic EPI calculation rather than to offer a detailed site characterization.

3. METHODOLOGY

The evaluation paradigm draws on prior deterministic methodologies utilized in nuclear plants [16], in which liquefaction consequences were predominantly evaluated using settlement-based criteria. However, such approaches do not explicitly address the probabilistic treatment of pore pressure evolution and interlayer hydraulic gradients. The Probabilistic Ejecta Potential Index (Prob_EPI) created in this study offers a systematic alternative that incorporates both aleatory and epistemic uncertainty into a physics-based model of sediment ejecta generation.

3.1 Probabilistic Ejecta Potential Index

This approach provides the Probabilistic Ejecta Potential Index (EPI) method as a new alternative for assessing the potential for liquefaction hazards based on the mechanism of sediment ejecta caused by high pore water pressure. Unlike the empirical Liquefaction Potential Index (LPI) [17], the EPI is formulated quantitatively by calculating the area of excess pore water pressure below the hydrostatic reference line (*hA*) along the saturated soil depth profile. The probabilistic relationship is based on a comparison of the EPI region and the Hydro-Mechanical Boundary (HMB) zone, which is established at the lower limit of 80% of the Hydro-Mechanical Boundary Line distribution (HMBL)[18]. The drawing of the HMB line which is assumed to be the soil liquefiable layer area is scientifically known at the initial boundary identified groundwater flow (on the y-axis) up to a depth of 30 m from the investigated soil layer. As a novelty, the proposed EPI model accommodates variations in the recurrence period of 250–5000 years so that the EPI probability can be calculated under different earthquake severity conditions. The implementation is based on a scenario-based hazard assessment [16]. This method allows for the spatial-temporal integration of pore pressure distributions for risk estimation. This approach is expected to address the limitations of the LPI, which ignores the actual pore water pressure distribution.

Mathematically, the EPI is defined as the squared integral of the difference between the maximum excess head (hexc) and hA over depth and time:

$$Prob\_EPI = \sum_{k=1}^{n-1} \frac{EPI}{HMB} \quad (1)$$

The Prob_EPI value ranges from 0 to 1, showing the percentage likelihood of a liquefaction event occurring, with 1 indicating a probability of 100%. The EPI (Excess Pore Pressure Index) parameter measures the area affected by excess pore pressure in square meters (m²), whereas the HMB refers to the area of the soil layer with the potential for liquefaction (liquefiable soil layer), also measured in m².

The area is calculated by integrating the space between two pore pressure curves against the depth z, as indicated in equation 1. As a novel methodology, this work recommends changing the basic equation with the discrete trapezoidal integration method described in equations 2 and 3. The goal of this approach is to improve the accuracy of EPI and HMB area estimation while also allowing for systematic probability correction. Depth discretization is performed in n segments [19] as expressed in Equation (2)

$$EPI_{base}\ (m^3.s) = \int_{t_0}^{t_f} \int_{z_0}^{z_{GWL}} (h_{exc} - h_A)^2 dz dt \quad (2)$$

$$EPI_{base} = \sum_{k=1}^{n-1} \frac{1}{2}(z_{k+1}) \left[\left(h_{exc}(z_k) - h_A(z_k) + \left(h_{exc}(z_{k+1}) - h_A(z_{k+1}) \right) \right) \right]^2$$

$$HMB_{base}\ (m^3.s) = \int_{t_0}^{t_f} \int_{z_0}^{z_{GWL}} (h_{exc} - h_{HMBL})^2 dz dt \quad (3)$$

$$HMB_{base} = \sum_{k=1}^{n-1} \frac{1}{2}(z_{k+1}) \left[\left(h_{exc}(z_k) - h_{HMBL}(z_k) + \left(h_{exc}(z_{k+1}) - h_{HMBL}(z_{k+1}) \right) \right) \right]^2$$

Where h_{exc} is the Maximum Excess Head, h_A is a diagonal reference line with a slope of H:V = 1:1 (one horizontal, one vertical) that represents the actual condition of pore water pressure during the earthquake, z_{GWL} is the depth of the groundwater table, t_0 and t_f are the time limit between the onset of acceleration 0.05 g and the maximum duration, and h_{HMBL} is the groundwater pressure in the easily liquefied layer. The EPI_{base} area of EPI has not been updated from the initial data. HMB_{base} denotes the uncorrected base area of HMB. A correction factor is added to scale the deterministic EPI values into probabilistic terms with the aim to compensate for the probabilistic behavior of ejecta occurrence. Both aleatory fluctuation in seismic demand and epistemic uncertainty in subsurface parameters are taken into consideration by this component. The following is the expression for the corrected probability of ejecta occurrence (*Prob EPI*)

$$Prob\ EPI = \frac{EPI_{\ base}}{HMB_{\ base}} \quad (4)$$

or in other words

$$Prob\ EPI = \frac{\sum_{k=1}^{n-1} \frac{1}{2}(z_{k+1}) \left[\left(h_{exc}(z_k) - h_A(z_k) + \left(h_{exc}(z_{k+1}) - h_A(z_{k+1}) \right) \right) \right]^2}{\sum_{k=1}^{n-1} \frac{1}{2}(z_{k+1}) \left[\left(h_{exc}(z_k) - h_{HMBL}(z_k) + \left(h_{exc}(z_{k+1}) - h_{HMBL}(z_{k+1}) \right) \right) \right]^2}$$

where $h_{exc}(z)$ denotes the excess pore-water head at depth z, $h_A(z)$ represents the artesian reference boundary, and $h_{HMBL}(z)$ indicates the hydraulic–mechanical boundary limit. z_k and z_{k+1} are the discrete depth increments used for trapezoidal integration. The resulting Prob_EPI value ranges between 0 and 1, signifying the probability level associated with ejecta occurrence — higher values indicating greater hydraulic connectivity and ejecta potential.

3.2 Validation of the Probability EPI Equation

To evaluate the sensitivity and accuracy of the HMBL threshold, a quantitative analysis was conducted using various statistical methods and data distribution distance measures. These include Cross/Pearson - Correlation, Dynamic Time Warping (DTW), Area Difference, Kullback–Leibler Divergence (KLD) dan Hellinger Distance. The validation compared model outputs across several threshold scenarios ranging from 50% to

90% of the hA value, aiming to determine the most representative proportion of the actual pore-pressure response for probabilistic EPI estimation. A detailed description of the implementation and interpretation of each metric is presented in the following paragraph.

Each statistical and distance-based measure served a distinct function in validating the probabilistic EPI formulation. Cross/Pearson Correlation, was employed to quantify the linear similarity between the modeled and reference pore-pressure responses, while Dynamic Time Warping (DTW) accounted for potential phase shifts along the depth profile. The Area Difference metric, provided a measure of cumulative deviation between the two curves, emphasizing overall energy consistency. In contrast, Kullback–Leibler Divergence (KLD) and Hellinger Distance evaluated the statistical proximity between the modeled and observed data distributions. Together, these metrics ensured that both the temporal and probabilistic characteristics of the pore-pressure field were consistently represented across different HMBL threshold scenarios

a. Pearson Correlation

The Pearson Correlation Coefficient is a statistical measure that determines the degree and direction of a linear relationship between two numerical variables. The Pearson correlation coefficient is used in signal and temporal data analysis to determine the similarity of patterns between two signals in the absence of time changes The purpose of this measure is to assess the linear relationship between two datasets, with outputs ranging from -1 (perfect negative correlation), 0 (no correlation), to 1 (perfect positive correlation). The mathematical equation is:

$$\rho(X,Y) = \frac{Cov(X,Y)}{\sigma_X \sigma_Y} \tag{5}$$

where ρ(X,Y) is the Pearson correlation, Cov(X,Y) is the covariance between X and Y, and σ_X and σ_Y are the standard deviations of each variable. This coefficient is widely used in model validation, variable dependency analysis, and correlation studies between signals in various disciplines. The use of Pearson correlation in the context of signal processing and statistical systems.

b. Dynamic Time Warping (DTW)

Dynamic Time Warping (DTW) is a well-known algorithm for calculating the similarity of two time series that may differ in length or have temporal misalignment [20]. DTW has been particularly beneficial in sensitivity analysis of dynamic systems, as it identifies temporal shifts in patterns caused by changes in input parameters. In essence, DTW depicts how a system's reaction varies when the timing of occurrences changes, even if the general shape of the patterns remains constant. The mathematical formula for DTW is as follows:

$$DTW\ (X,Y) = \min \sum_{(i,j)\in P} d(x_i, y_j) \tag{6}$$

where $d(x_i, y_j)$ is the distance between elements $x_i\ dan\ y_j$, and P is the optimization path that minimizes the total distance. DTW searches for the best matching path (P) between two sequences x and y that minimizes the sum of the distances between elements $x_i\ dan\ y_j$. This distance is usually calculated using the Euclidean distance. DTW is used to compare two data sequences that can be of different lengths.

c. Area Difference

In sensitivity analysis, the area difference between the response curves of a reference dataset and a test dataset can be used to evaluate the impact of input parameter variations on the model output. This method quantifies the extent to which changes in input parameters affect the shape and area under the response curve, thereby reflecting the model's sensitivity to such variations. Mathematically, the area difference (ΔA) between two response curves, f(x) and g(x), over the interval [a,b], can be calculated using the following equation:

$$\Delta A = \int_a^b |f(x) - g(x)|\, dx \tag{7}$$

where f(x) and g(x) are functions that represent the model's response to input parameters on the reference dataset and the test dataset, respectively. This integral measures the total area difference between the two curves over a specified interval.

The area difference approach is commonly used in sensitivity analysis to determine how changes in input parameters affect model responses. This method, one of the established approaches in global sensitivity analysis, makes it easier to identify crucial parameters that have a large impact on model results [21]. Its efficacy stems from its ability to quantify the extent to which changes in inputs affect the model's response surface, making it an invaluable tool for model calibration, validation, and interpretation. As a result, area difference analysis provides a solid foundation for understanding model behavior in the presence of parameter uncertainty.

d. Kullback–Leibler Divergence

In sensitivity analysis, the Kullback–Leibler Divergence (KLD) is employed to quantify the

extent to which a model's output distribution is altered by variations in input parameters. By measuring the divergence between two probability distributions, KLD provides a probabilistic metric that captures the magnitude of change in the output response. A higher KLD value indicates greater sensitivity of the system to the respective parameter variation. Mathematically, the KLD between two probability distributions, $P(i)$ and $Q(i)$, is defined as follows:

$$D_{KL}(P \,||\, Q) = \sum_i P(i) \log\left(\frac{P(i)}{Q(i)}\right) \quad (8)$$

In this context, $P(i)$ represents the model output distribution with modified input parameters, while $Q(i)$ reflects the distribution based on reference inputs. A higher Kullback–Leibler Divergence (KLD) indicates that input changes significantly alter the output distribution, suggesting high model sensitivity. KLD has been used to assess the influence of different priors on posterior distributions in autoregressive time series models [22]. It has also been applied to identify consistent parameter estimates in Kalman filter frameworks by comparing posterior distributions from various initial parameters [23]. These examples highlight KLD as an effective metric for evaluating how input variations impact model behavior, supporting better calibration and validation.

e. Hellinger Distance

Hellinger Distance is a metric used to quantify the similarity between two probability distributions. Unlike other measures such as Kullback-Leibler Divergence, Hellinger Distance is symmetric and bounded between 0 and 1, where 0 indicates identical distributions and 1 represents completely distinct ones. It is mathematically defined as follows:

$$H(P,Q) = \frac{1}{2}\sqrt{\sum_i \left(\sqrt{p(x)} - \sqrt{q(x)}\right)^2 dx} \quad (9)$$

In Equation (9), $H(P,Q)$ denotes the Hellinger Distance between the modeled probability distribution P and the reference distribution Q. $p(x)$ and $q(x)$ are the corresponding probability density functions at depth increment x, and the summation is performed over all discrete observations i. The term dx represents the sampling interval, while the factor ½ ensures normalization such that $H(P,Q)$ ranges from 0 (identical distributions) to 1 (completely dissimilar). Hellinger Distance is used to measure the spatial distribution differences in probabilistic data modeling, such as in seismic applications. Its relevance lies in its stability against small data fluctuations and its ability to handle zero probability values without causing singularities.

f. Jensen-Shannon Divergence (JSD)

Jensen–Shannon Divergence (JSD) is a symmetric and finite information-theoretic metric for measuring the similarity between two probability distributions P and Q. It is defined as:

$$D_{JS}(P\|Q) = \frac{1}{2}D_{KL}(P\|Q) + \frac{1}{2}D_{KL}(Q\|M) \quad (10)$$
$$where\ M = \frac{1}{2}(P+Q)$$

Here, D_{KL} denotes the Kullback–Leibler divergence, and M is the average (mixture) distribution of P and Q, JSD is bounded between 0 (identical distributions) and 1 (maximally different), depending on the logarithmic base. This property makes it especially suitable for applications in clustering, topic modeling, and generative model evaluation.

The six similarity indicators were carefully chosen to provide complementary viewpoints on the concordance between modeled and observed pore pressure responses. Pearson Correlation (CC) represents linear similarity, Dynamic Time Warping (DTW) reveals temporal misalignment, and Area Difference (AD) measures overall variance in curve amplitude and shape. Meanwhile, Kullback-Leibler Divergence (KLD) and Jensen-Shannon Divergence (JSD) are information-theoretic indicators of distributional divergence, with JSD offering a symmetric and bounded alternative. Finally, Hellinger Distance (HD) is a stable and symmetric measure of similarity that is resistant to tiny variations. By using these six measures combined, both curve-based (time-depth dependent) and distribution-based (probabilistic) consistencies can be evaluated, reduce epistemic bias in the calibration process.

The application of thresholds ranging from 50% to 90% of the reference line (hA) is intended to indicate various degrees of conservatism. Lower thresholds (50-60%) may catch more likely liquefaction manifestations but risk overestimation, whereas higher thresholds (80-90%) use stricter criteria to minimize false positives but may underestimate danger severity. This approach gives a balanced interpretation of liquefaction risk that may be customized for site-specific engineering safety requirements.

It should also be noted that the current validation methodology does not currently support full aleatory uncertainty propagation using stochastic or Monte Carlo ground motion simulations. Although Prob_EPI is naturally probabilistic due to the EPI/HMB ratio, future developments ought to include stochastic ground motion ensembles to explicitly reflect variability over repetition periods and soil stratigraphies. This

change would make the Prob_EPI approach more durable and feasible in probabilistic seismic hazard analysis (PSHA). This multi-metric validation ensures that the proposed Prob_EPI equation integrates both linear and nonlinear similarities, temporal alignment, and distributional consistency, improving the liquefaction hazard assessment.

Figure **2** depicts the whole methodological framework. The flowchart describes the sequential stages, which include input data preparation, excess pore pressure computation, reference and HMBL definition, probabilistic scaling, validation with six statistical measures, threshold sensitivity analysis, and final calibration for practical application.

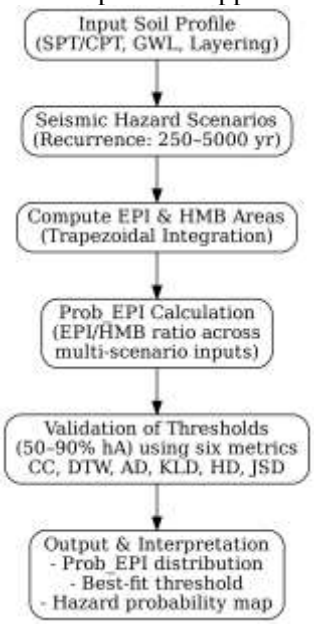

Figure 2. Flowchart of the Probabilistic Ejecta Potential Index (Prob_EPI) methodology

4. RESULTS AND DISCUSSION

The Prob_EPI formulation was derived using the DH11 and DH17 datasets; however, the validation process employed the DH09 profile because it provides a more continuous and complete pore-pressure record. Both boreholes are located within the same stratigraphic unit and share similar hydraulic and geotechnical properties, ensuring that the DH09-based validation remains fully representative of the DH17-derived model.

4.1. Serpong DH 11

The potential for ejecta at the study site was evaluated using the Ejecta Potential Index (EPI), which is derived from the difference between the maximum excess pore pressure head and total effective stress at various depths. Positive and significant EPI values indicate critical zones where excess pore pressure is large enough to trigger soil particle mobilization to the surface or the occurrence of ejecta phenomena, particularly in saturated layers undergoing decompression due to seismic wave propagation.

The presented figure 3 shows the 2D Ejecta Potential Index (EPI) profile for borehole DH11 in Serpong, covering five earthquake return periods: 250, 500, 1000, 2500, and 5000 years. Each subplot illustrates the variation of Maximum Excess Head (MEH) with depth, along with curves for maximum pore pressure, total stress, effective stress, and the EPI-positive zone (highlighted in light blue). Table 3 presents the EPI and sediment ejecta probability calculations for different return periods, offering crucial information on the soil's seismic response at the Serpong DH11 site. The data shows an increasing trend in EPI area with longer return periods. At a 250-year return period, the EPI area is 64.875 m², rising to 75.959 m² at 5000 years. This indicates that as seismic load increases (reflected by longer return periods), the area of soil with excess pore pressure exceeding the effective stress also grows. Moreover, the EPI probability consistently increases from 0.200 (20.003%) at 250 years to 0.243 (24.314%) at 5000 years, reflecting a higher potential for soil ejecta with more extreme earthquake scenarios. The total analyzed area also increases from 89.345 m² to 108.600 m², likely representing the depth or area coverage considered in the vertical soil profile..

The 2D profile plot reinforces these findings, with each subplot displaying the vertical soil profile and mapping the Max Excess Head and Effective Stress curves, along with the EPI area shaded in blue. For each return period, the EPI area consistently forms between the Excess Head and Effective Stress curves, with its size steadily increasing across the different scenarios. This EPI area represents zones where pore water pressure exceeds effective stress, indicating the potential for ejecta due to seismic events (Figure 3).

Technically, the graph shows that the EPI zone is concentrated between depths of 6 to 22 meters across all return periods. This suggests that the critical soil layer for ejecta remains relatively constant vertically, with the EPI area expanding mainly horizontally due to increased Excess Head. The Effective Stress curve remains stable with depth, while the Excess Head curve shifts right (increases) with longer return periods. This shift enlarges the intersection between the Excess Head and Effective Stress curves, directly increasing the EPI value.

The vertical thickness of the EPI area remains relatively constant, indicating that the thickness of

the soil layer susceptible to excess pore pressure does not increase with higher earthquake intensity, but rather, the intensity of pore pressure itself increases. Visually, the EPI area expands to the right, reflecting the higher pore pressure resulting from stronger seismic excitation. However, this becomes clearer when compared to the geotechnical characteristics from the soil profile data (Table 3). The site is predominantly composed of sand and gravelly sand layers (2.8 m to 14.8 m depth), followed by clayey sand and silty clay layers to 30 m. The sand layers (SP) exhibit moderate relative density (Dr ≈ 45–46%) and high initial shear modulus (Go ≈ 2000–2250 kPa), but with very low permeability (k ≈ 10^{-5} to 10^{-6} m/s), indicating a significant potential for pore pressure accumulation during seismic excitation. In contrast, deeper layers like Silty Clay have higher permeability but lower shear modulus. Interestingly, despite the increase in excess pore pressure with longer return periods, the EPI zone consistently remains within the sand layers. This suggests that the mechanical and hydraulic properties of the low-permeability, moderately dense sand layers are the primary factors driving the sensitivity to excess pore pressure. In other words, the underlying soil characteristics of the EPI zone remain relatively unchanged, meaning that while EPI values and areas increase, their vertical distribution remains stable. Based on the data from the table, graph, and soil characterization, it can be concluded that the potential for soil ejecta at the study site consistently increases with longer return periods. However, this increase is primarily driven by soil layers that are inherently susceptible to excess pore pressure. This pattern is critical for foundation design and stability assessments in areas considered for strategic development sites, such as nuclear power plant locations, where low-density, low-permeability sand layers are a key concern.

Table 3: EPI Calculations and Probabilities at Serpong DH11.

Return Period	EPI (m2)	Total Area - HMB (m2)	Probability of EPI	ProbabilityEPI (%)
250	17.872	89.345	0.200	20.003
500	18.958	93.813	0.210	21.003
1000	19.906	98.503	0.221	22.053
2500	20.901	103.428	0.232	23.156
5000	21.946	108.600	0.243	24.314

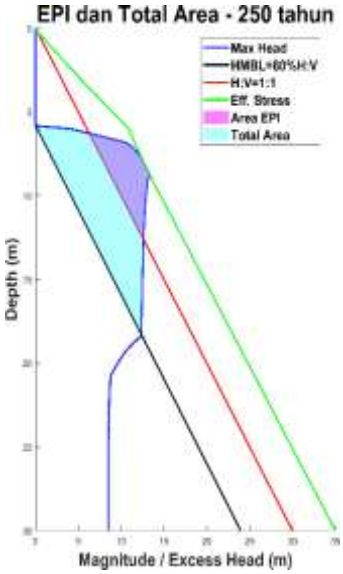

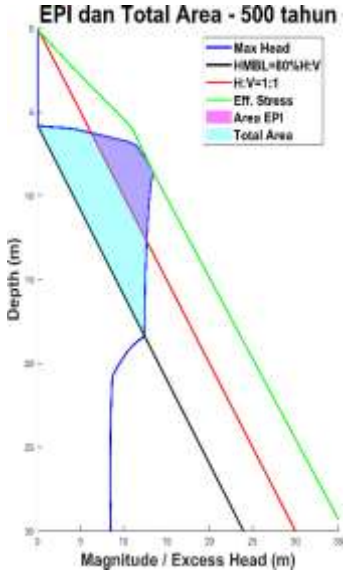

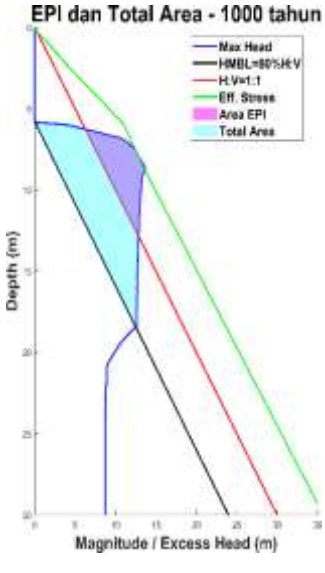

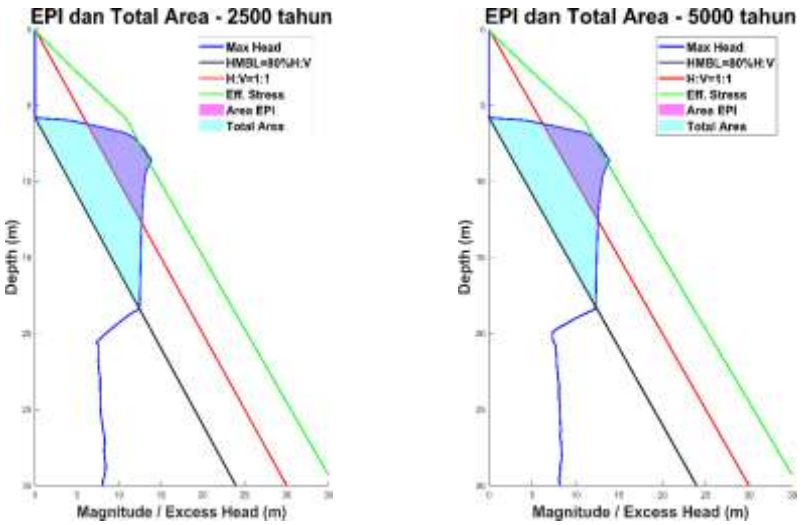

Figure 3: 2D Ejecta Potential Index Profile for the Serpong area at DH11, showing variations in soil shaking levels for return periods of 250, 500, 1000, 2500, and 5000 years

4.2 Serpong DH 17

The data reveals a significant increasing trend in both the Ejecta Potential Index (EPI) area and its probability with longer earthquake return periods. The EPI area sharply rises from 10,981 m² at a 250-year return period to a peak of 70,568 m² at 2500 years, indicating an expansion of the soil zone experiencing excess pore pressure due to increased seismic load. However, at the 5000-year return period, there is a slight decrease in the EPI area to 67,489 m², despite an increase in the total Hydro-Mechanical Boundary (HMB) area. This phenomenon suggests that, in extreme earthquake scenarios, pore pressure distribution in the soil extends to greater depths, but does not always correlate with a proportional horizontal expansion of the ejecta zone.

The 2D vertical profile visualization illustrates the evolution of excess pore pressure and critical boundaries with depth for each return period scenario. The blue zone representing the EPI area expands both laterally and vertically, particularly for return periods between 500 and 2500 years (Table 4 and Figure 4). This increase indicates that excess pore pressure not only rises in absolute terms but also extends to greater soil depths. The proportional changes in the Max Head, Excess Head, and Effective Stress parameters across earthquake load scenarios further strengthen the correlation between seismic intensity and the potential ejecta zone.

.The critical EPI zone consistently lies between depths of 5 to 17 meters, corresponding to the Gravelly Sand and Clayey Sand layers. At this depth, there is an overlap between the Excess Head and Effective Stress curves with the HMB boundary, indicating the accumulation of maximum pore pressure and the minimum soil bearing capacity. While deeper layers, such as Sandy Clay and Silty Clay (>20 m depth), exhibit relatively high shear modulus and low permeability, their contribution to the ejecta zone is smaller, as they are better able to maintain stability under seismic loading. Therefore, a thorough understanding of the soil's physical properties is crucial for evaluating the potential for soil failure due to earthquakes. The 5–17 m depth zone is identified as the most vulnerable to ejecta, making it a critical focus for seismic hazard assessment.

Tabel 4. The result caltulation of EPI and Probabiliy EPI at Serpong DH17

Return Period	EPI (m2)	Total Area - HMB (m2)	Probability EPI	Probability EPI (%)
250	3.0032	43.103	0.070	6.967
500	10.628	70.850	0.150	15.001
1000	16.482	85.492	0.193	19.279
2500	19.465	91.480	0.213	21.278
5000	20.004	96.054	0.223	22.341

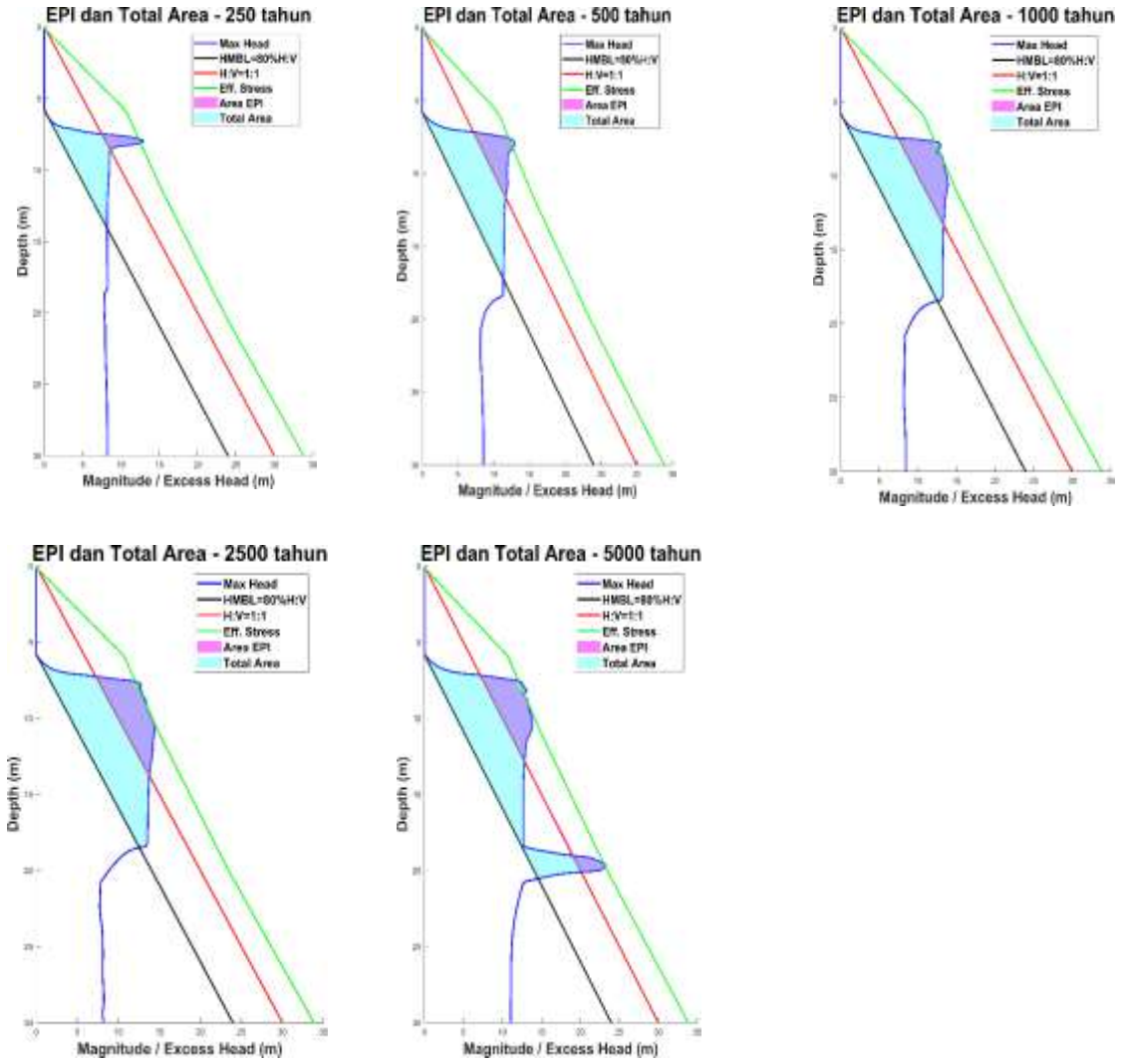

Figure 4. The 2D Ejecta Potential Index Profile for the Serpong area at DH17, showing variations in soil shaking levels for return periods of 250, 500, 1000, 2500, and 5000 years

Figure 5 shows comparison tables of EPI and Prob_EPI for DH11 and DH17. While both sites display an increasing trend with return period, DH17 has significantly higher sensitivity in Prob_EPI. This disparity is not just a numerical difference; it is entrenched in the geotechnical context. DH11 is underlain by interbedded silty sand layers with limited permeability, which limits excess pore pressure migration and consequently ejecta potential even when liquefaction occurs at a depth. In contrast, DH17 has thicker, cleaner sandy deposits with better permeability, resulting in stronger upward hydraulic gradients. This stratigraphic disparity explains why Prob_EPI at DH17 increases rapidly with increasing return period, whereas DH11 grows more slowly.

a)

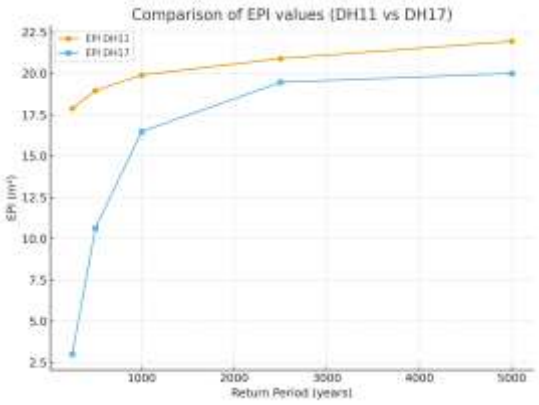

b)

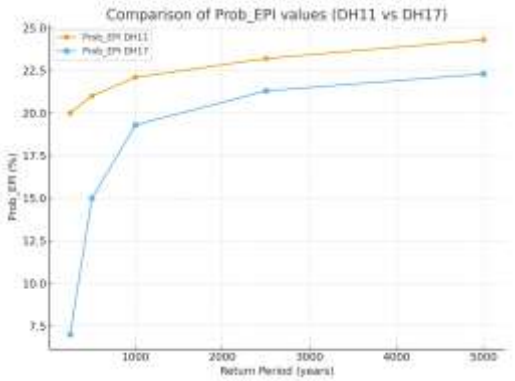

Figure 5. Compilation of comparation tables of EPI, Prob EPI for DH1 and DH17 in various return period

4.3. Validation of Hydro-Mechanical Boundary (HMB) Delineation

The delineation of the Hydro-Mechanical Boundary (HMB) is a critical step in calculating the Probabilistic Ejecta Potential Index (Prob_EPI), as it defines the maximum depth of hydraulically active, liquefiable soil that contributes to sediment ejecta under excess pore pressure. In this study, the HMB was determined based on the percentage of maximum pore pressure head, with threshold variations ranging from 50% to 90% of a reference head value (hA), aligned with a 1:1 hydraulic gradient (H:V). To assess the reliability of the HMB as the lower boundary of the excess pore pressure zone, a quantitative validation was performed using six statistical similarity metrics: Cross-Correlation (CC), Dynamic Time Warping (DTW), Area Difference (AD), Kullback–Leibler Divergence (KLD), Jensen–Shannon Divergence (JSD), and Hellinger Distance (HD). This validation was applied to four borehole sites: DH11 and DH09 (Serpong), and two additional sites in Carita and Palu (Figure 6).

The evaluation results at borehole DH11 are presented in Table 5 and Figure 7. All threshold scenarios yielded a Pearson correlation coefficient (CC) of 1.0, indicating identical overall curve shapes. However, more sensitive metrics such as Dynamic Time Warping (DTW) and Hellinger Distance (HD) revealed that the 80% threshold line (X3–Y3) produced the lowest deviation, with DTW = 6.74×10^{-17} and HD = 4.58×10^{-33}. These values demonstrate a statistically close alignment with the reference gradient line (H:V = 1:1), although the 80% line does not intersect the effective stress boundary, as observed in the 90% threshold scenario. Visually (Figure 7), the 80% line also best follows the shape of the reference gradient without excessive overlap into non-liquefiable zones.

The evaluation at the Carita borehole (Table 6 and Figure 8) exhibited a similar pattern. The 80% HMB threshold offered the best compromise between shape conformity (DTW = 3.47×10^{-17}) and physical realism, avoiding overlap with the effective stress boundary. Although the 90% threshold yielded numerically perfect similarity (DTW and HD = 0), it lacks physical representativeness, as it aligns directly with the effective stress line rather than the pore pressure gradient. At the DH09 site in Serpong, the results (Table 7 and Figure 9) further reinforce the finding that the 80% HMB threshold yields exceptionally low statistical metrics (DTW = 4.19×10^{-17}; HD = 3.23×10^{-33}) while maintaining separation from the effective stress curve. This supports its functional relevance as the lower boundary of the excess pore pressure zone (EPI > 0). A similar trend was observed at the Palu site (Table 8 and Figure 10). Although the 90% threshold line achieved perfect numerical similarity (DTW and HD = 0), the 80% line was preferred due to its lack of significant overlap with the effective stress boundary, rendering it more applicable to realistic stratigraphic systems.

Overall, both statistical and visual evaluations across all four sites confirm that the 80% HMB threshold offers an optimal balance between statistical validity and geotechnical interpretability. This threshold effectively delineates the distribution of excess pore pressure relevant to sediment ejecta hazards, without compromising the physical meaning of the EPI. Accordingly, the 80% HMB line is recommended as a reliable lower boundary for liquefiable soil layers in Prob_EPI calculations and as a reference for liquefaction risk zonation at critical infrastructure sites.

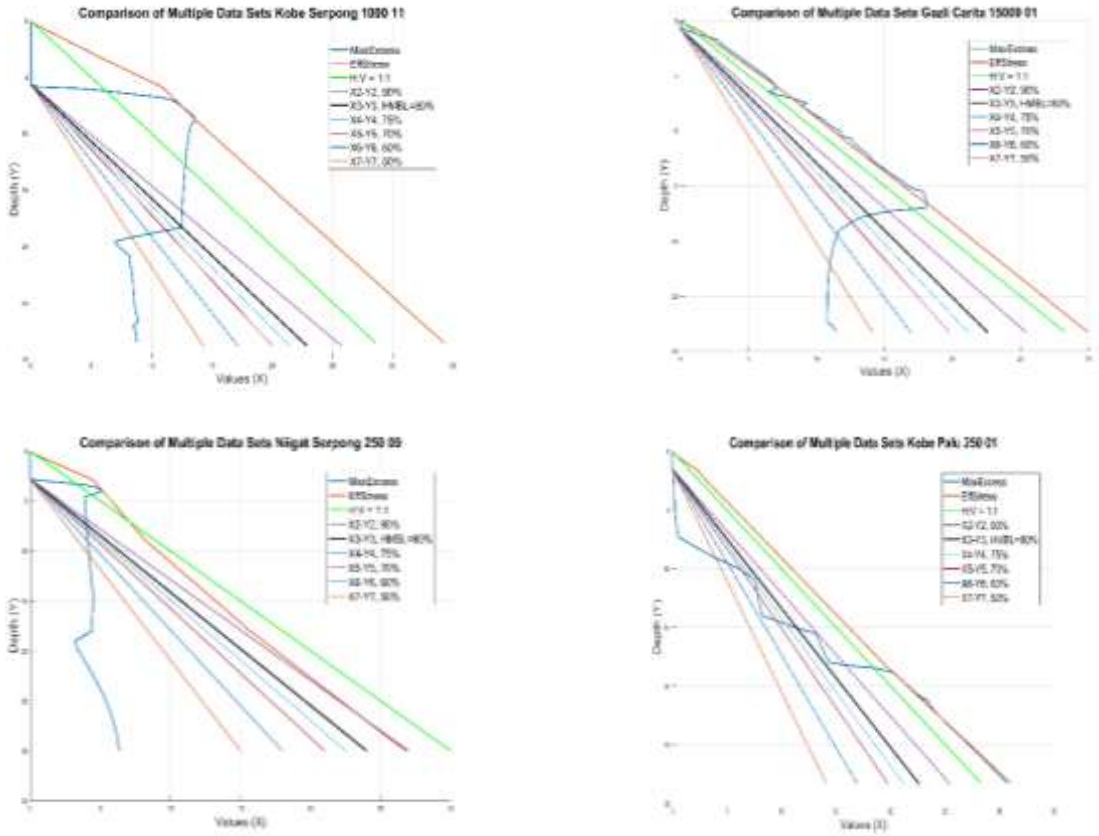

Figure 6. Distribution of EPI and comparison curves for various threshold-based HMB lines (50–90%) against the reference H:V = 1:1 gradient at Borehole DH11, Serpong.

Table 5. Statistical similarity metrics comparing the reference H:V = 1:1 curve with varying threshold lines (50–90%) for HMB delineation at DH11, Serpong.

Dataset	CC	DTW	AD	KLD	JSD	HLD
50%	1	7.08899E-17	0.058328259	0	-9.46724E-19	3.57602E-33
60%	1	1.94723E-16	0.058328259	0	1.17166E-17	1.40801E-32
70%	1	9.92621E-17	0.054332434	0	1.30997E-17	6.88805E-33
75%	1	1.7714E-16	0.058328348	0	1.24527E-17	9.24467E-33
80%	1	6.74264E-17	0.058328259	0	2.45021E-18	4.58607E-33
90%	1	0	0.058328289	0	0	0

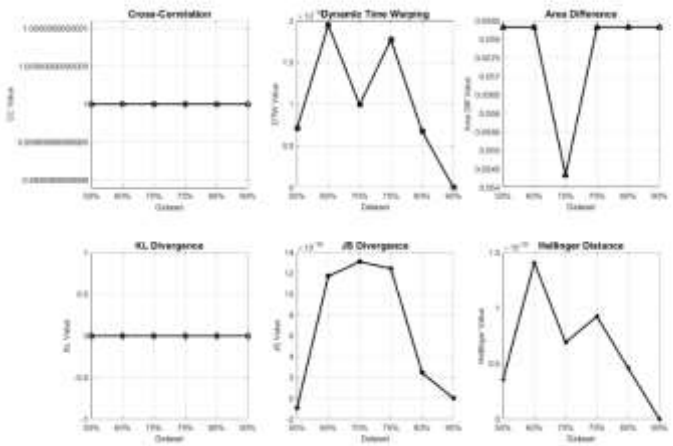

Figure 7. Statistical evaluation using six similarity metrics for threshold-based HMB curves (50–90%) compared to the reference H:V = 1:1 line at DH11, Serpong.

Table 6. Statistical similarity assessment between the reference H:V = 1:1 gradient and HMB curves (50–90%) using six evaluation metrics at DH01, Carita.

Dataset	CC	DTW	AD	KLD	JSD	HD
50%	1	2.04103E-16	0.007929486	2.26533E-16	1.6162E-17	1.10502E-32
60%	1	1.3653E-16	0.00792957	1.53184E-16	4.66096E-18	6.64747E-33
70%	1	5.29091E-17	0.00792957	9.75452E-18	7.71388E-18	2.85986E-33
75%	1	1.80874E-16	0.007929542	1.98939E-16	1.76397E-17	1.18651E-32
80%	1	3.47216E-17	0.00792957	1.93834E-17	1.2609E-18	1.84359E-33
90%	1	0	0.00792957	0	0	0

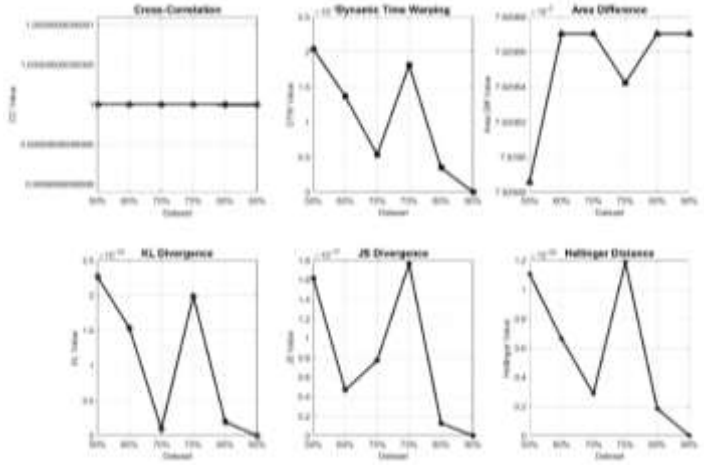

Figure 8. Statistical evaluation using six similarity metrics for threshold-based HMB curves (50–90%) compared to the reference H:V = 1:1 line at DH01 Carita

Table 7. Statistical similarity assessment between the reference H:V = 1:1 gradient and HMB curves (50–90%) using six evaluation metrics at DH09, Serpong

Dataset	CC	DTW	AD	KLD	JSD	HD
50%	1	7.88029E-17	0.027972026	5.18075E-17	3.74685E-18	4.42079E-33
60%	1	1.34148E-16	0.027972044	0	8.49111E-19	7.70343E-33
70%	1	8.08815E-17	0.027972053	0	2.72203E-19	5.66865E-33
75%	1	8.54673E-17	0.027972008	6.50607E-17	2.12029E-17	5.29641E-33
80%	1	4.1907E-17	0.027972008	4.37795E-18	2.8876E-18	3.23274E-33
90%	1	0	0.027971978	0	0	0

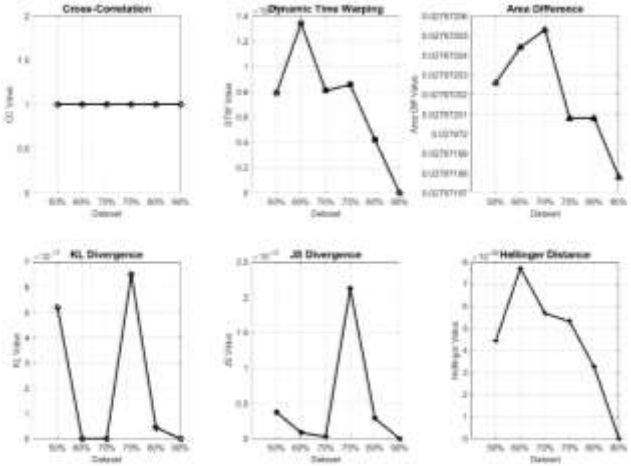

Figure 9. Statistical evaluation using six similarity metrics for threshold-based HMB curves (50–90%) compared to the reference H:V = 1:1 line at DH09 Serpong

Table 8. Statistical similarity assessment between the reference H:V = 1:1 gradient and HMB curves (50–90%) using six evaluation metrics at DH01, Palu

Dataset	CC	DTW	AD	KLD	JSD	HD
50%	1	2.04103E-16	0.015859254	2.26533E-16	1.6162E-17	1.10502E-32
60%	1	1.3653E-16	0.015859141	1.53184E-16	4.66096E-18	6.64747E-33
70%	1	5.29091E-17	0.015859846	9.75452E-18	7.71388E-18	2.85986E-33
75%	1	1.80874E-16	0.015859189	1.98939E-16	1.76397E-17	1.18651E-32
80%	1	3.47216E-17	0.015859084	1.93834E-17	1.2609E-18	1.84359E-33
90%	1	0	0.015859141	0	0	0

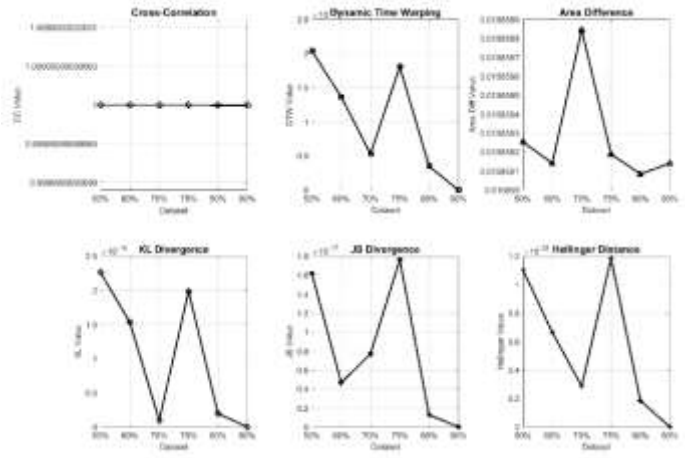

Figure 10. Statistical evaluation using six similarity metrics for threshold-based HMB curves (50–90%) compared to the reference H: V = 1:1 line at DH01 Palu

Although a direct benchmarking with LPI and LSN at DH11 and DH17 was not performed in this study, it is worth noting that these indices, derived from CSR–CRR relationships, are generally reported in the literature to increase monotonically with seismic demand and return period. In contrast, Prob_EPI represents a probabilistic measure that directly accounts for pore pressure migration and hydraulic gradients. Thus, while the comparison here is conceptual rather than numerical, the key distinction is that Prob_EPI provides outcomes in probabilistic terms, which are more consistent with probabilistic safety assessment frameworks for NPP siting. In summary, while direct numerical benchmarking with LPI and LSN was not conducted for DH11 and DH17, the conceptual comparison highlights the methodological distinction between probabilistic and deterministic severity indices. This conceptual linkage provides a broader context for interpreting the Prob_EPI results and positions the method within the continuum of liquefaction hazard assessment tools. Building upon this understanding, the next section discusses the engineering implications of the Prob_EPI findings for nuclear power plant siting and possible ground improvement measures.

From an engineering perspective, the differentiated response between DH11 and DH17 carries direct implications for site mitigation strategies. At DH17, the rapid increase of Prob_EPI underscores the necessity of targeted ground improvement measures such as vertical drains, stone columns, or permeation grouting to dissipate pore pressures and mitigate ejecta risk. By contrast, the lower sensitivity observed at DH11 suggests a comparatively higher site suitability, requiring less intensive interventions. These insights demonstrate that Prob_EPI does not merely correlate conceptually with traditional indices but, more importantly, refines hazard assessment by explicitly incorporating permeability effects. This enables more rational engineering decisions in nuclear power plant (NPP) siting and provides a probabilistic framework directly compatible with Probabilistic Safety Assessment (PSA) practices.

Furthermore, the Prob_EPI results show that probabilistic scaling of the Ejecta Potential Index can improve the site-specific assessment of liquefaction-induced ejecta hazards in accordance with international nuclear siting guidelines [24]. Compared to the deterministic technique used at the Paks Nuclear Power Plant [16], this paradigm allows for explicit quantification of uncertainty and more robust safety margins in beyond-design-basis seismic scenarios.

5. CONCLUSION

This study introduces the probabilistic Excess Pore Pressure Index (Prob_EPI = EPI/HMB) as the first physics-based framework applied to liquefaction hazard assessment for nuclear power plant (NPP) site characterization in Indonesia. By explicitly capturing the spatial and temporal distribution of excess pore pressure, Prob_EPI advances beyond conventional indices such as LPI and LSN, offering a more physically grounded and probabilistic quantification of sediment ejecta potential. Application to boreholes DH11 and DH17 demonstrates that Prob_EPI systematically increases with longer earthquake return periods, with liquefaction-prone zones concentrated at depths of 5–22 meters. Validation through six statistical similarity metrics confirmed the robustness of an 80% Hydro-Mechanical Boundary (HMB) threshold as a reliable criterion for delineating liquefiable soil layers.

From an engineering perspective, Prob_EPI provides regulators and design engineers with a practical decision-support tool for evaluating liquefaction hazard in critical infrastructure planning. Its integration of seismic uncertainty, soil stratigraphy, and pore pressure dynamics makes it particularly suited to guide NPP site selection, safety margin definition, and risk-informed design. By delivering a site-specific and physics-based hazard index, this approach bridges the gap between geotechnical modeling and regulatory requirements, ensuring that liquefaction hazard analysis contributes directly to engineering solutions for long-term nuclear safety.

Future research should expand the framework through several directions: (i) incorporating three-dimensional numerical simulations to capture lateral pore pressure migration and ejecta pathways, (ii) applying Monte Carlo and other stochastic simulations to represent uncertainty in seismic input, soil variability, and model parameters, and (iii) conducting multi-site validation across diverse geological settings. Integration with probabilistic seismic hazard analysis (PSHA) will further strengthen the method's robustness. These developments will enhance Prob_EPI into a pioneering, scalable, and scientifically rigorous index for liquefaction hazard assessment in NPP site characterization and other high-stakes engineering applications.

ACKNOWLEDGMENT (Optional)

This publication is part of the doctoral research conducted under the Degree by Research (DBR) Program in Civil Engineering, Faculty of Engineering, Universitas Indonesia, with full funding and support from the National Research and Innovation Agency (BRIN). The authors gratefully acknowledge BRIN for providing the doctoral scholarship and research facilities.

AUTHOR CONTRIBUTION

Akhmad Muktaf Haifani : Conceptualization, Methodology, Formal analysis, Data curation, Software, Visualization, Writing – Original Draft, Project administration. Hadi Suntoko: Supervision, Resources, Validation, Investigation (site-specific geology hazard context). Topan Setiadipura: Funding acquisition, Supervision, Writing – Review & Editing, Data interpretation (nuclear site safety relevance). Widjojo A. Prakoso: Supervision, Methodological guidance, Writing – Review & Editing, Technical validation (geotechnical modeling).

REFERRENCES

1. Bray F., R., Olaya, J., D. "2022 H. Bolton Seed Memorial Lecture: Evaluating Liquefaction Effects," *J. Geotech. Geoenvironmental Eng.*, vol. 149, no. 8, p. 03023002, 2023, doi: https://doi.org/10.1061/JGGEFK.GTENG-11242.
2. Ding T., Zhang Y., Liu, G., and Yang Y., "Experimental Study of Liquefaction Strength Affected by Residual Excess Pore Water Pressure Induced by Earthquake," *Japanese Geotech. Soc. Spec. Publ.*, vol. 10, no. 21, pp. 786–790, 2024, doi: 10.3208/jgssp.v10.os-10-06.
3. Green B., Cubrinovski R., A., Cox M., Wood B., Wotherspoon C., Bradley L., & Maurer B., "Select liquefaction Case Histories from the 2010–2011 Canterbury Earthquake Sequence. Earthquake Spectra," *Earthq. Spectra*, vol. 30, no. 1, pp. 131-153., 2014, doi: https://doi.org/10.1193/030713EQS066M.
4. Boulanger R., W., and Idriss I., M., "CPT and SPT Based Liquefaction Triggering Procedures, Report UCD/CGM-10/2," *Cent. Geotech. Model*, no. April, pp. 1–138, 2014.
5. Van Ballegooy C., H., S., Malan P., Lacrosse V., Jacka M. E., Cubrinovski M., Bray J. D., "Assessment of Liquefaction-induced Land Damage for Residential Christchurch.," *Earthq. spectra*, vol. 30, no. 1, pp. 31-55., 2014, doi: https://doi.org/10.1193/031813EQS070M.
6. Hutabarat J,. D., & Bray D., "Effective Stress Analysis of Liquefiable Sites to Estimate the Severity of Sediment Ejecta," *J. Geotech. Geoenvironmental Eng. 147(5), 04021024.*,

vol. 147, no. 5, p. 04021024., 2021, doi: https://doi.org/10.1061/(ASCE)GT.1943-5606.0002503.
7. Maurer B. A., Green B., W., Cubrinovski R., A. & Bradley M., "Evaluation of the Liquefaction Potential Index for Assessing Liquefaction Hazard in Christchurch, New Zealand.," *J. Geotech. Geoenvironmental Eng.*, vol. 147, no. 5, p. 04021024., 2014.
8. Bray J., D., and Hutabarat D., "CPT-based Liquefaction Ejecta Evaluation Procedure," *Cone Penetration Test. 2022 - Proc. 5th Int. Symp. Cone Penetration Testing, CPT 2022*, no. 2016, pp. 844–849, 2022, doi: 10.1201/9781003308829-125.
9. Yang X., Zhang Y., and Li Z., "Embankment Displacement PLAXIS Simulation and Microstructural Behavior of Treated-Coal Gangue," 2020. doi: 10.3390/min10030218.
10. Cubrinovski M., *et al.*, "Geotechnical Aspects of the 22 February 2011 Christchurch Earthquake," *Bull. New Zeal. Soc. Earthq. Eng.*, vol. 44, no. 4, pp. 205–226, 2011, doi: 10.5459/bnzsee.44.4.205-226.
11. Bray J., & Macedo J. D. "6th Ishihara lecture: Simplified Procedure for Estimating Liquefaction-induced Building Settlement," *Soil Dyn. Earthq. Eng.*, vol. 102, pp. 215–231, 2017, doi: https://doi.org/10.1016/j.soildyn.2017.08.026.
12. IAEA, "Seismic Hazard Assessment in Site Evaluation for Nuclear Installations: Ground Motion Prediction Equations and Site Response [Internet]. Vienna: International Atomic Energy Agency," 2016.
13. USNRC, "Site Safety Analysis Report Standard Review Plan: Liquefaction Hazard Evaluation," 2015.
14. János Katona T., Győri E., Bán Z., and Tóth L., "Assessment of Liquefaction Consequences for Nuclear Power Plant Paks," *Transactions*, no. Iaea 2017, p. 23, 2015.
15. BATAN, "Site Evaluation Report of RDE on Seismic Aspect," Jakarta, 2016.
16. Katona T., J., Bán Z., Gyori E., Tóth L., and Mahler A., "Safety Assessment of Nuclear Power Plants for Liquefaction Consequences," *Sci. Technol. Nucl. Install.*, vol. 2015, 2015, doi: 10.1155/2015/727291.
17. Boulanger R., W., and Idriss I., M., "CPT-Based Liquefaction Triggering Procedure," *J. Geotech. Geoenvironmental Eng.*, vol. 142, no. 2, pp. 1–11, 2016, doi: 10.1061/(asce)gt.1943-5606.0001388.
18. Cubrinovski M., Rhodes A., Ntritsos N., and Van Ballegooy S., "System Response of Liquefiable Deposits," *Soil Dyn. Earthq. Eng.*, vol. 124, no. April 2018, pp. 212–229, 2019, doi: 10.1016/j.soildyn.2018.05.013.
19. Das B., M., *Advanced Soil Mechanics, Fifth Edition*, 5th Edition. London: CRC Press, 2019. doi: https://doi.org/10.1201/9781351215183.
20. Fortela M., E., Mikolajczyk D., L., Hernandez A., P., Revellame R., Sharp E., Holmes W., Zappi W., "Dynamic Time Warping as Elementary Effects Metric for Morris-Based Global Sensitivity Analysis of High-Dimension," *Dyn. Model. Math. Comput. Appl.*, vol. 29, no. 6, p. 111, 2024.
21. Saltelli S., Ratto A., Andres M., Campolongo T., Cariboni F., Gatelli J., Tarantola D., "Sensitivity Analysis: A Review of Recent Advances," *Eur. J. Oper. Res.*, vol. 248, no. 3, 2015, doi: https://doi.org/10.1016/j.ejor.2015.06.032, 869-887.
22. Amin A., A., "Kullback–Leibler Divergence to Evaluate Posterior Sensitivity to Different Priors for Autoregressive Time Series," *Commun. Stat. - Simul. Comput. 48(5), 1277–1291.*, vol. 48, no. 5, pp. 1277–1291, 2019, doi: https://doi.org/10.1080/03610918.2017.
23. Impraimakis M., "A Kullback–Leibler Divergence Method for Input–system–state Identification," *J. Sound Vib.*, vol. 569, p. 117965., 2024, doi: https://doi.org/10.1016/j.jsv.2023.117965.
24. IAEA, "Site Evaluation for Ninstallations: Safety Requirements (IAEA Safety Standards Series No. SSR-1)," 2016.